AXISYMMETRIC STAGNATION-POINT FLOW AND HEAT TRANSFER OF NANO-FLUID IMPINGING ON A CYLINDER WITH CONSTANT WALL HEAT FLUX

Hamid MOHAMMADIUN[1], Vahid AMERIAN [2], Mohammad MOHAMMADIUN [3], Iman KHAZAEE[4], Mohsen DARABI[*5] and Mohammadreza ZAHEDI[5]

[1]*Assistant Professor, Department of mechanical engineering, Shahrood branch, Islamic Azad University, Shahrood, Iran.*

[2]*Department of mechanical engineering, Shahrood University, Shahrood, Iran.*

[3]*Associate Professor, Department of mechanical engineering, Shahrood branch, Islamic Azad University, Shahrood, Iran.*

[4]*Assistant Professor, Faculty of Mechanical and Energy Engineering, Shahid Beheshti University, A.C., Tehran, Iran.*

[5]*Young Researchers and Elite Club, Shahrood Branch, Islamic Azad University, Shahrood, Iran*

[*] Corresponding author; E-mail**:** mdarabi514@gmail.com

The steady-state, viscous flow and heat transfer of Nano-fluid in the vicinity of an axisymmetric stagnation point of a stationary cylinder with constant wall haet flux is investigated. The impinging free-stream is steady and with a constant strain rate $\bar{k}$ *. Exact solution of the Navier–Stokes equations and energy equation are derived in this problem. A reduction of these equations is obtained by use of appropriate transformations introduced in this research. The general self-similar solution is obtained when the wall heat flux of the cylinder is constant. All the solutions above are presented for Reynolds numbers* $\mathrm{Re} = \frac{\bar{k}a^2}{2\upsilon_f}$ *ranging from 0.1 to 1000, selected values of heat flux and selected values of particle fractions where* a *is cylinder radius and* υ_f *is kinematic viscosity of the base fluid. For all Reynolds numbers, as the particle fraction increases, the depth of diffusion of the fluid velocity field in radial direction, the depth of the diffusion of the fluid velocity field in* z *-direction, shear-stresses and pressure function decreases. However, the depth of diffusion of the thermal boundary layer increases. It's clear by adding nanoparticles to the base fluid there is a significant enhancement in Nusselt Number and heat transfer.*

KEYWORDS: *Nano-fluid , Stagnation-point flow, heat transfer, Nusselt number, stationary cylinder, self-similar solution.*

NOMENCLATURE

ρ_n	Nano-fluid density	u	Radial component of velocity field
ϕ_v	Particle fraction	w	Axial component of velocity field
ρ_f	Base fluid density	σ	Shear stress

ρ_p	Particle density	P	Dimensionless pressure
d_f	Equivalent diameter of a base fluid molecule	f	Dimensionless function
d_p	Equivalent diameter of a particle molecule	υ_n	Kinematic viscosity of nano-fluid
μ_n	Dynamic viscosity of the nano-fluid	m	Shape factor
μ	Dynamic viscosity of the base fluid	k_{eff}	Thermal conductivity of nano-fluid
η	Similarity variable	T_{fr}	The freezing point unit of the base fluid
Re_n	Nano-fluid Reynolds number	Re_P	Nanoparticle Reynolds number
Re	Base fluid Reynolds number	Pr_b	Base fluid Prandtl number
$\bar{k}$	Strain rate of free stream	h	Convective heat transfer coefficient
a	Radius of the cylinder	Nu	Nusselt number
r, z	Cylindrical coordinates	q_w	Wall heat flux
υ_f	Kinematic viscosity of base fluid	θ	Dimensionless Temperature

1- INTRODUCTION

In recent years, many researchers have been performed to study the effects of nano-fluid on convective heat transfer rate. M. Sheikholeslami and Shehzad, [1] reported the Numerical analysis of Fe3O4–H2O nanofluid flow in permeable media under the effect of external magnetic source. Sheikholeslami et al. [2] has obtained the numerical solution for nano-fluid Electrohydrodynamic flow and natural convection heat transfer in a porous medium. Also they considered thermal radiation term in energy equation. In other research Sheikholeslami investigated the homogeneous nano-fluid flow and forced convection heat transfer inside a lid driven porous cavity [3]. In this work influence of Lorentz forces and Shape effect of nanoparticle on nan-ofluid MHD forced convection have been considered and Temperature distribution and flow style have been presented for various values of Hartmann, Darcy and Reynolds numbers.

Sheikholeslami [4] presented Numerical simulation for heat transfer intensification of nano-fluid in a porous curved enclosure considering shape effect of Fe3O4 nanoparticles Sheikholeslami [5] reported Magnetic field influence on nano-fluid thermal radiation in a cavity with tilted elliptic inner cylinder.

The history of the analytical methods studies using similarity solution techniques goes back to Hiemenz [6]. Wang [7] was first who found exact solution for the problem of axisymmetric stagnation flow on an infinite stationary circular cylinder. Gorla[8-11] in a series of papers, studied the steady and unsteady flows over a circular cylinder in the vicinity of the stagnation-point for the cases of constant axial movement, and the special case of axial harmonic motion of a non-rotating cylinder. This special case is only for small and high values of frequency parameter using perturbation techniques.

Mohammadiun et al. [12] have investigated the Stagnation-Point Flow and Heat Transfer of a Viscous, Compressible Fluid on a Cylinder, and in the next study the problem of stagnation point flow and heat transfer of compressible fluid impinging on a moving cylinder has been considered by them [13]. They continued their investigation by solving the problem of stagnation point flow of a nano fluid on stationary cylinder when the wall temperature of the cylinder was constant [14].

MHD mixed convection slip flow near a stagnation-point on a nonlinearly vertical stretching sheet in the presence of viscous dissipation has been considered by shateyi and mabood [15]..

Mahmood et al[16] has been discussed the time-dependent axisymmetric stagnation-point flow and heat transfer of a viscous fluid over a disc lubricated with power-law fluid. The

aim of their study was to investigate the influence of slip parameter and unsteadiness parameter on the flow characteristics and heat transfer.

Amirsom et al. [17] presented the similarity solution of governing equations for the magneto convective stagnation point flow of bionano-fluid with melting heat transfer. A lattice Boltzmann model of nano-fluid flow boiling in a tube has been established by yao et al [18]. They simulated the effect of different bubble distances and lateral accelerations *a* on the bubble growth process and the effect of heat transfer.

In the present analysis, for the first time the similarity solution of the heat transfer enhancement of steady viscous flow of nano-fluid in the vicinity of an axisymmetric stagnation point of a stationary cylinder with constant heat flux is considered. It is interesting to note that in current work the thermal conductivity coefficient of nano-fluid is considered temperature-dependent and the ordinary differential equation has been derived. Flow is considered in cylindrical coordinates (*r*,*z*) with corresponding velocity components (*u*,*w*), as Fig. 1. The laminar steady incompressible flow of Nano-fluid in the neighborhood of an axisymmetric stagnation-point of a stationary cylinder is considered.

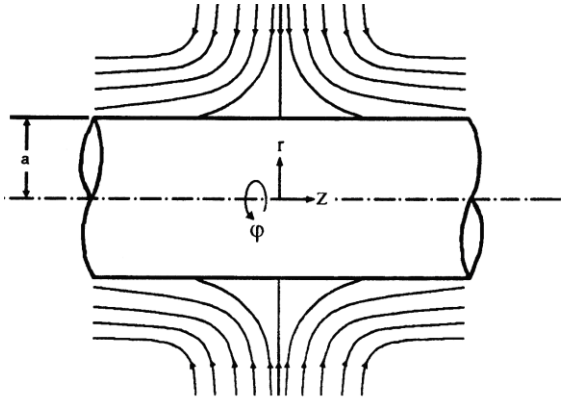

Fig. 1. Schematic diagram of a stationary cylinder

2-PROPERTIES OF NANO-FLUID

The aluminum oxide (γAl_2O_3) nanoparticles which have been used in this research have the following characteristics:

Density $\rho_m = 3600$ kg/m^3, mean particle diameter is 44 nm.

2-1- DENSITY

We will assume that the density of the aluminum oxide nanoparticles is constant in the entire range of considered temperature. The following relation has been used to compute the nano-fluid density:

$$\rho_n = (1-\phi_v)\rho_f + \phi_v \rho_p \qquad (1)$$

Where subscripts *n*, *f* and *p* denote the nano-fluid , base fluid and the particles respectively, and ϕ_v is the particle fraction.

2-2- DYNAMIC VISCOSITY

Massimo Corcione proposed empirical correlation for predicting the relative viscosity, [19]

$$\frac{\mu_n}{\mu} = \frac{1}{1 - 34.87(\frac{d_p}{d_f})^{-0.3} \phi_v^{1.03}} \quad (2)$$

Where d_f is the equivalent diameter of a base fluid molecule, given by

$$d_f = 0.1(\frac{6M}{N\pi\rho_{f0}})^{\frac{1}{3}} \quad (3)$$

In which *M* is the molecular weight of the base liquid, *N* is the Avogadro number, and ρ_{f0} is the mass density of the base liquid calculated at temperature $T_0 = 293k$.

Different values used in this formula are mentioned in table 1.

In this research Corcione's formula has been used to extract the Navier-stocks equations.

2-3-THERMAL CONDUCTIVITY

Two different models have been used to determine the thermal conductivity coefficient of nano-fluid.

2-3-1- Model 1:

Massimo Corcione[19] proposed empirical correlation for predicting the effective thermal conductivity based on a high number of experimental data available in the literature. It is found that, for given the nanoparticle material and the base fluid, the ratio between the thermal conductivities of the nano-fluid and the pure base liquid increases as the nanoparticle volume fraction and the temperature are increased, and the nanoparticle diameter is decreased. The ease of application of the equations proposed, and their wide regions of validity for the thermal conductivity data, make such equations useful by the engineering point of view, for both numerical simulation purposes and thermal design tasks.

$$\frac{k_{eff}}{k_f} = 1 + 4.4\,\mathrm{Re}_p^{\,0.4}\,\mathrm{Pr}_{bf}^{\,0.66}(\frac{T}{T_{fr}})^{10}(\frac{k_p}{k_f})^{0.03}\phi_v^{\,0.66} \quad (4)$$

Where T_{fr} is the freezing point unit of the base fluid. Also Re_p and Pr_{bf} are the nanoparticle Reynolds number and the base fluid Prandtl number, respectively, which presented below

$$\mathrm{Re}_p = \frac{2\rho_{bf}k_bT}{\pi\mu_{bf}^{\,2}d_p} \quad \text{and} \quad \mathrm{Pr}_{bf} = \frac{\mu_{bf}(c_p)_{bf}}{k_{bf}} \quad (5)$$

In equation (5), k_b is the Boltzmann's constant equal to 1.38066×10^{-23} J/K. Finally, the Corcione's correlation, which is temperature-dependent correlation, has been used to extract the Energy equation.

2-3-2- Model 2:

In model (2) thermal conductivity coefficient of nano-fluid has been expressed by following relation [2,3]:

$$\frac{k_{eff}}{k_f} = \frac{-m(k_f - k_p)\emptyset_v + (k_p - k_f)\emptyset_v + mk_f + k_p + k_f}{mk_f + (k_f - k_p)\emptyset_v + k_f + k_p} \quad (6)$$

Values of shape factors for various shapes of nanoparticles are presented in Table 2.

3- PROBLEM FORMULATION

The laminar steady incompressible flow of nano-fluid in the neighborhood of an axisymmetric stagnation-point of a stationary cylinder has been considered. The Navier-Stokes and energy equations in cylindrical coordinates governing the axisymmetric flow are given by [7-11]:

Mass,

$$\frac{\partial}{\partial r}(r u)+r\frac{\partial w}{\partial z}=0 \tag{7}$$

Momentum,

$$u\frac{\partial u}{\partial r}+w\frac{\partial u}{\partial z}=-\frac{1}{\rho_n}\frac{\partial p}{\partial r}+\upsilon_n(\frac{\partial^2 u}{\partial r^2}+\frac{1}{r}\frac{\partial u}{\partial r}-\frac{u}{r^2}+\frac{\partial^2 u}{\partial z^2}) \tag{8}$$

$$u\frac{\partial w}{\partial r}+w\frac{\partial w}{\partial z}=-\frac{1}{\rho_n}\frac{\partial p}{\partial z}+\upsilon_n(\frac{\partial^2 w}{\partial r^2}+\frac{1}{r}\frac{\partial w}{\partial r}+\frac{\partial^2 w}{\partial z^2}) \tag{9}$$

And Energy,

$$\frac{1}{r}\frac{\partial}{\partial r}(rk_{eff}\frac{\partial T}{\partial r})+\frac{\partial}{\partial z}(k_{eff}\frac{\partial T}{\partial z})=(\rho c_p)_n[u\frac{\partial T}{\partial r}+w\frac{\partial T}{\partial z}] \tag{10}$$

The boundary conditions for velocity field are:

$$r=a:\quad u=0\quad,\quad w=0 \tag{11}$$

$$r\to\infty:\ u=-\bar{k}\,(r-\frac{a^2}{r})\quad,\quad w=2\bar{k}\,z \tag{12}$$

In which, (11) are no-slip conditions on the cylinder wall and relations (12) show that the viscous flow solution approaches, in an analogous manner to the Hiemenz flow, the potential flow solution as $r\to\infty$. For the temperature field, we have

$$\begin{cases} r=a: & q=q_w=cons\tan t \\ r\to\infty: & T\to T_\infty \end{cases} \tag{13}$$

Where q_w is the wall heat flux, respectively, and T_∞ is the freestream temperature.

A reduction of the Navier-Stokes equations is obtained by the following coordinate separation of the velocity field which is actually modeled by the form of their limits as represented by Equation (14):

$$u=-\bar{k}\frac{a}{\sqrt{\eta+1}}f(\eta)\ ,\ w=2\bar{k}\,f'(\eta)z\ ,\ p=\rho_n\bar{k}^2a^2P \tag{14}$$

Where $\eta=(\frac{r}{a})^2-1$ is dimensionless radial variable and prime denotes differentiation with respect to η. Transformations (14) satisfy (7) automatically and their insertion into (8) – (10) yields an ordinary differential equation in terms of $f(\eta)$, and an expression for the pressure:

$$(\eta+1)f'''+f''+\mathrm{Re}_n[1-(f')^2+f\,f'']=0 \tag{15}$$

$$P-P_0=-[\frac{f^2(\eta)}{2(\eta+1)}+\frac{1}{\mathrm{Re}_n}f'(\eta)]-2(\frac{z}{a})^2 \tag{16}$$

In these equations,

$$\mathrm{Re}_n = \beta \frac{\bar{k}\, a^2}{2\upsilon_f} \tag{17}$$

$$\beta = [1 - 34.87(\frac{d_p}{d_f})^{-0.3} \phi_v^{1.03}](1 - \phi_v + \phi_v \frac{\rho_p}{\rho_f}) \tag{18}$$

And Re_n is the Reynolds number for nano-fluid . From conditions (11) and (12), the boundary conditions for (14) are as follows:

$$\begin{aligned} &\eta = 0: \quad f = 0, \quad f' = 0 \\ &\eta \to \infty: \quad f' = 1 \end{aligned} \tag{19}$$

To transform the energy equation into a nondimensional form, we introduce

$$\theta(\eta) = \frac{T(\eta) - T_\infty}{\frac{a\, q_w}{2 k_{bf}}} \tag{20}$$

By using Corcione's correlation and introducing Γ as

$$\Gamma = 4.4(\frac{2\rho_{bf} K_b}{\pi \mu_{bf}\, d_p^{\,2}})^{0.4} \frac{1}{T_{fr}^{\,10}} (\frac{k_p}{k_f})^{0.03} \tag{21}$$

The energy equation can be written as

$$\begin{aligned} &\left\{1 + \Gamma \phi_v^{\,0.66}\, \mathrm{Pr}_{bf}^{\,0.66} [T_\infty + \frac{a\, q_w}{2 k_{bf}} \theta]^{10.4}\right\} [(\eta + 1)\theta'' + \theta'] + 10.4 [T_\infty + \frac{a\, q_w}{2 k_{bf}} \theta]^{9.4} \\ &\frac{a\, q_w}{2 k_{bf}} \Gamma \phi_v^{\,0.66}\, \mathrm{Pr}_{bf}^{\,0.66} (\eta + 1)(\theta')^2 + \left\{1 - \phi_v + \phi_v [\frac{(\rho c_p)_p}{(\rho c_p)_f}]\right\} \mathrm{Re}_{bf}\, \mathrm{Pr}_{bf}\, f\theta' = 0 \end{aligned} \tag{22}$$

Using model (2) of thermal conductivity coefficient leads to following relation for energy equation:

$$(\eta + 1)\theta'' + \theta' + \mathrm{Re}_n\, \mathrm{Pr}_{nf}\, f\theta' = 0 \tag{23}$$

From condition (13), the boundary conditions for (22) and (23) are as follow:

$$\begin{cases} \eta = 0: & -\frac{k_{nf}}{k_{bf}} \theta'(0) = 1 \\ \eta \to \infty: & \theta(\infty) = 0 \end{cases} \tag{24}$$

Equations (15), (22) and (23) along with boundary conditions (19) and (24) have been solved by using the finite difference method along with *TDMA* algorithm [20]. Using this method, the initial values were guessed and the iteration was repeated until the convergence was obtained. In these computations the grid size was chosen 0.001 and the truncation error was set at 1E-9.

The flowchart of numerical method was depicted in the Appendix

4- NUSSELT NUMBER

The Nusselt number has been presented by the following relations:

$$\theta(0) = \frac{T_w - T_\infty}{\frac{a\, q_w}{2 k_{bf}}} \;\&\; h = \frac{q_w}{T_w - T_\infty} \to Nu = \frac{h\, a}{2 k_{bf}} = \frac{1}{\theta(0)} \tag{25}$$

5- SHEAR-STRESS

The shear-stress on the surface of the cylinder is obtained from:

$$\sigma = \mu_n [\frac{\partial w}{\partial r}]_{r=a} \tag{26}$$

Where μ_n is viscosity of the nano-fluid . Using definition (14), the shear-stress at the cylinder wall for self-similar solutions becomes

$$\sigma = \mu_n [2\bar{k}\, f''(0)\, z]\frac{2}{a} \quad \Rightarrow \quad \frac{\sigma a}{4\mu_n \bar{k}\, z} = f''(0) \tag{27}$$

6- RESULTS AND DISCUSSIONS

In this section, the solution of the ordinary differential equations (15) and (22), for prescribed values of surface heat flux and selected values of Reynolds numbers and particle volume fraction are presented.

Sample profiles of the $f(\eta)$ function against η at $\phi_v = 0.02$ and for selected values of Reynolds numbers are presented in Fig. 2. Since with the increase of Reynolds number the dynamic inertia forces overcome the viscosities forces, as expected like the behavior of the base fluid, the depth of diffusion of the momentum increases. So as the Reynolds number increases, the depth of diffusion of the fluid velocity field in radial direction increases, too.

Effects of variation of particle Volume fraction factor on $f(\eta)$ function against η and selected value of Reynolds number Re=1000 is shown in Fig. 3. Since any increase of ϕ_v leads to an increase in dynamic viscosity, the resistance of the viscos forces against the dynamic inertia forces increases. It is interesting to note that as ϕ_v increases the depth of diffusion of the fluid velocity field in radial direction decreases. So, for all the Reynolds numbers, the base fluid case produces the highest value of radial velocity and as particle Volume fraction increases, this quantity decreases accordingly.

Sample profiles of the $f'(\eta)$ function against η for $\phi_v = 0.02$, and for selected values of Reynolds numbers are shown in Fig. 4. Again as Reynolds number increases, the depth of diffusion of the fluid velocity field in z - direction increases, too.

Effects of variations of particle Volume fraction factor on $f'(\eta)$ function against η for selected value of Reynolds number Re=0.1 are shown in Fig.5. It is interesting to note that as ϕ_v increases the depth of the diffusion of the fluid velocity field in z -direction also decreases. Again, the base fluid case ($\phi_v = 0$) produces the highest value of velocity in z -direction and as particle Volume fraction factor increases, this quantity decreases accordingly.

Sample profiles of the $\theta(\eta)$ function against η for the case of constant wall heat flux for $\phi_v = 0.05$, $\frac{a\, q_w}{2\, k_{bf}} = 200$, and for selected values of Reynolds numbers are depicted in Fig. 6. As expected, the momentum is increased with the Reynolds number and consequently, not only the thermal boundary layer thickness is decreased once the thermal diffusion is overcome, but also the wall dimensionless temperature is decreased, as can be observed in the following figures.

Effect of variations of particle fraction factor on $\theta(\eta)$ function against η for, $\frac{a\, q_w}{2\, k_{bf}} =$ constant, and selected values of Reynolds numbers are presented in Figs.7-8. For $\phi_v = 0$, base fluid, the result of Gorla [21] is extracted; it is interesting to note that, as ϕ_v increases, the absolute value of the dimensionless temperature gradient is decreased at surfaces and the wall dimensionless temperature is decreased, too; nevertheless, this decreasing rate is negligible compared to that of the heat transfer coefficient. Therefore, the heat transfer coefficient is

increased through addition of nanoparticles.

Sample profiles of the dimensionless temperature $\theta(\eta)$ against η for $\phi_v = 0.05$ and Re=100, for selected values of heat flux are depicted in Fig. 9. As heat flux increases, the dimensionless temperature decreases and so does the temperature gradient at surface. It is evident that the absolute value of the dimensionless temperature gradient is decreased at surfaces; nevertheless, this decreasing rate is negligible compared to that of the heat transfer coefficient. Therefore, the Nusselt number is increased through addition of nanoparticles.

Effects of variations of particle fraction factor on Nusselt number against Reynolds number for selected values of wall heat flux are presented in Fig. 10. It is interesting to note that, as ϕ_v increases, the depth of the diffusion of the thermal boundary layer increases. Based on the figures, an increase in the heat flux and the Reynolds number along with addition of nanoparticles will result in increased heat transfer coefficient.

Effect of wall heat flux on Nusselt number against Reynolds number for selected values of variations of particle fraction factor is depicted in Fig.11. As it reveals in this figures, increase in heat flux results in decrease in dimensionless temperature at the surface, whereas Nusselt number has inverse relation with dimensionless temperature at surface, as heat flux increases Nusselt number increases as well. Generally more heat flux results in more temperature gradient at the surface, also forced heat convection increases same as the heat convection coefficient.

Sample profiles of non-dimensional temperature, derived by using Eq.25 for thermal conductivity are shown in fig. 12. As it is clear, both employed model in this research are showing same trend, which validates how useful the first model is. The profiles reveal that as shape factor increases, temperature at surface decreases. Whereas, considering reverse relation between Nuselt number and temperature, an increase in shape factor results in an increase in Nuselt number. Therefore, platelet particles are more effective than spherical ones in enhancement of heat transfer.

In fig. 13, effect of particle volume fraction on dimensionless temperature is shown. Sample profiles are plotted using Eq.25 for thermal conductivity. As it is expected, same as the trend in fig. 7 and 8, the more particle volume fraction, the less non-dimensional temperature at surface and consequently more Nuselt number.

7- CONCLUSIONS

A similarity solution for the Navier-Stokes equations and energy equation has been obtained for the problem of axisymmetric stagnation-point flow of a nano-fluid on a stationary cylinder with constant wall heat flux. A reduction of these equations is obtained by the use of appropriate transformations introduced for the first time. The general self-similar solution is obtained when the wall heat flux of the cylinder is constant. All the solutions above have been presented for Reynolds numbers, $\mathrm{Re} = \dfrac{\bar{k}a^2}{2\upsilon_f}$ ranging from 0.1 to 1000 and different values of particle Volume fraction ϕ_v. It can be said that for all Reynolds numbers and cylinder wall heat flux, as ϕ_v increases the depth of diffusion of the fluid velocity field in radial and axial directions decreases. But the Nusselt number and the depth of diffusion of the thermal boundary layer increases.

8- REFERENCES

[1] Sheikholeslami M and Shehzad S.A, Numerical analysis of Fe3O4–H2O nano-fluid flow in permeable media under the effect of external magnetic source, *International Journal of Heat and Mass Transfer*, 118 (2018), pp 182-192.

[2] Sheikholeslami M and Seyednezhad M, Simulation of nano-fluid flow and natural convection in a porous media under the influence of electric field using CVFEM, *International Journal of Heat and Mass Transfer*, 120 (2018), pp.772–781.

[3] Sheikholeslami M, CuO-water nano-fluid flow due to magnetic field inside a porous media considering Brownian motion, *Journal of Molecular Liquids*, 249 (2018), pp. 921-929.
[4] Sheikholeslami M, Shamlooei M, Moradi R, Numerical simulation for heat transfer intensification of nanofluid in a porous curved enclosure considering shape effect of Fe3O4 nanoparticles, *Chemical Engineering and Processing: Process Intensification*, 124 (2018), pp.71-82.
[5] Sheikholeslami M, Magnetic field influence on nanofluid thermal radiation in a cavity with tilted elliptic inner cylinder, *Journal of Molecular Liquids*, 229(2017), pp.137-147.
[6] Hiemenz K, Die Grenzchicht an einem in den gleichformingen Flussigkeitsstrom eingetauchten geraden, *Kreiszylinder. Dinglers Polytech. J*, 326 (1911), pp.321-410.
[7] Wang C, Axisymmetric stagnation flow on a cylinder. *Quarterly of Applied Mathematics*, 32(1974),2, pp.207-213.
[8] Gorla RSR, Unsteady laminar axisymmetric stagnation flow over a circular cylinder, *Dev. Mech*, 9(1977), pp.286-288.
[9] Gorla RSR, Nonsimilar axisymmetric stagnation flow on a moving cylinder, *Int. J. Engineering Science.* 16(1978), 6, pp.397-400.
[10] Gorla RSR, Transient response behavior of an axisymmetric stagnation flow on a circular cylinder due to time dependent free stream velocity, *Int. J. Engng. Sci*, 16 (1978),7, pp.493- 502.
[11] Gorla RSR, Unsteady viscous flow in the vicinity of an axisymmetric stagnation-point on a cylinder, *Int. J. Engng. Sci*, 17(1979), 1, pp.87-93.
[12] Mohammadiun H and Rahimi AB, Stagnation-Point Flow and Heat Transfer of a Viscous, Compressible Fluid on a Cylinder, *Journal of Thermophysics and Heat Transfer*, 26(2012), 3, pp.494-502.
[13] Rahimi AB, Mohammadiun H and Mohammadiun M, Axisymmetric stagnation flow and heat transfer of a compressible fluid impinging on a cylinder moving axially, *J. Heat Transfer*, 138(2016) ,2, 022201.
[14] Mohammadiun H, Amerin V, Mohammadiun M and Rahimi AB, Similarity Solution of Axisymmetric Stagnation-Point Flowand Heat Transfer of a Nano-fluid on a Stationary Cylinderwith Constant Wall Temperature, *Iran J Sci Technol Trans Mech Eng*, 41(2017) ,1, pp.91–95.
[15] Shateyi S and Mabood F, MHD mixed convection slip flow near a stagnation-point on a nonlinearly vertical stretching sheet in the presence of viscous dissipation, *Thermal Science*, (2015), 00, pp. 219-219.
[16] Mahmood K, Sajid M, Ali N and Javed T, Heat transfer analysis in the time-dependent axisymmetric stagnation point flow over a lubricated surface, *Thermal Science*, (2016), 00, pp. 257-257.
[17] Amirsom N, Uddin M. J, and Izani A, Electro magneto convective stagnation point flow of bionano-fluid with melting heat transfer and Stefan blowing, *Thermal Science*, (2017), 00, pp. 134-134.
[18] Shouguang Y, Tao H, Kai Z, Jianbang Z and Shuhua W, Simulation of flow boiling of nano-fluid in tube based on LBM, *Thermal Science*, (2017) , 00, pp. 6-6.
[19] Corcione M, Empirical-correlating equations for predicting the effective thermal conductivity and dynamic viscosity of nano-fluid s, *Ene. Convers. Manage*, 52(2011), 1, pp.789-793.
[20] Press WH, Flannery BP, Teukolsky SA and Vetterling WT, Numerical Recipes: The Art of Scientific Computing. Cambridge Univ. Press, New York, (1997), 548.
[21] Gorla RSR, Heat Transfer in an Axisymmetric Stagnation Flow on a Cylinder, *Applied Scientific Research*, 32(1976) ,5, pp.541– 553.

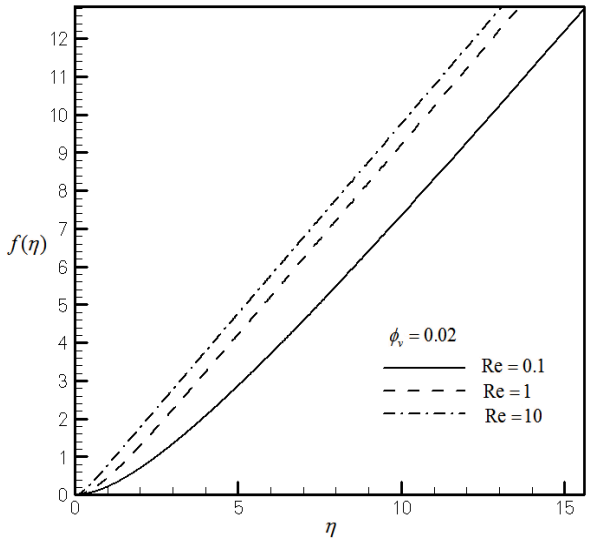

Fig. 2. Variation of f in terms of η at $\phi_v = 0.02$ for different values of Reynolds numbers

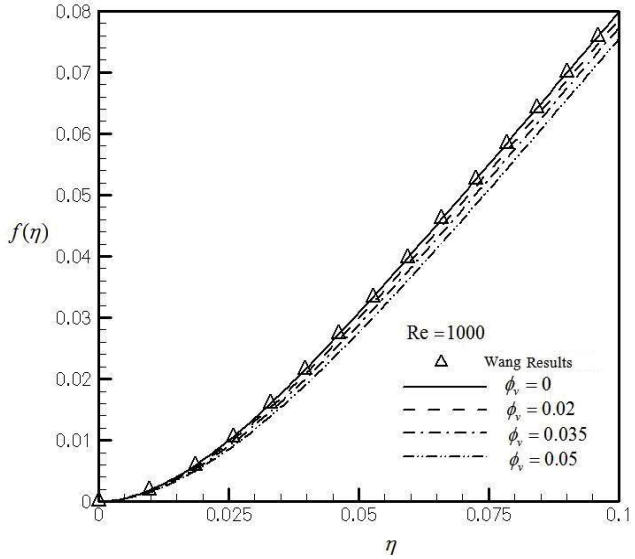

Fig. 3. Variation of f in terms of η at $\mathrm{Re} = 1000$ and for different values of particle volume fraction

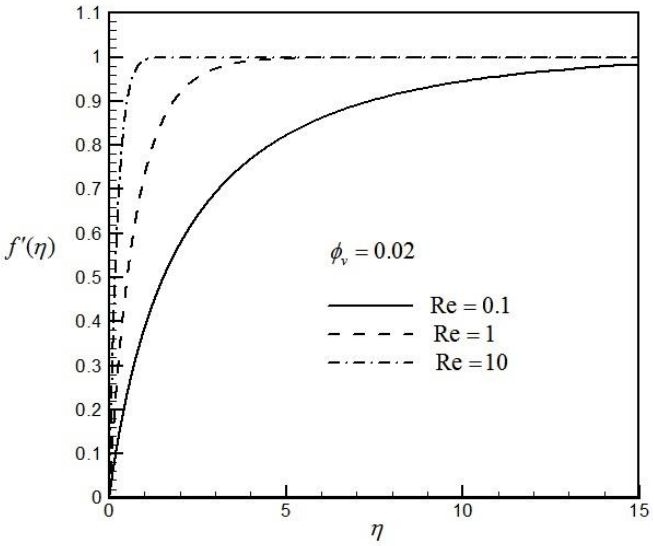

Fig. 4. Variation of f' in terms of η at $\phi_v = 0.02$ and for different values of Reynolds number

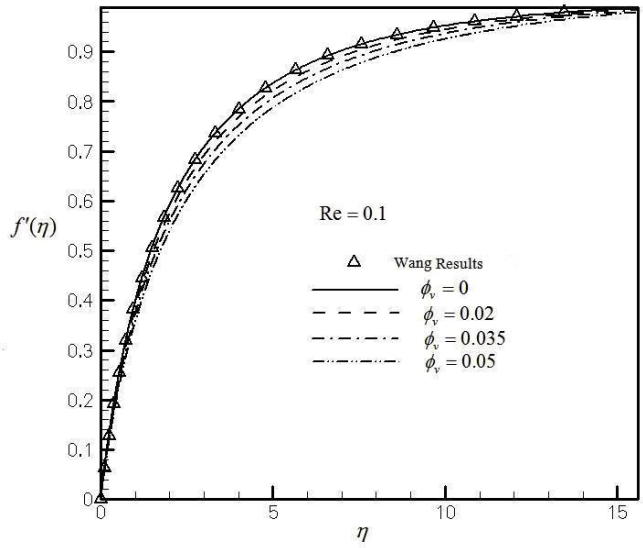

Fig. 5. Variation of f' in terms of η at $\mathrm{Re} = 0.1$ and for different values of particle volume fraction

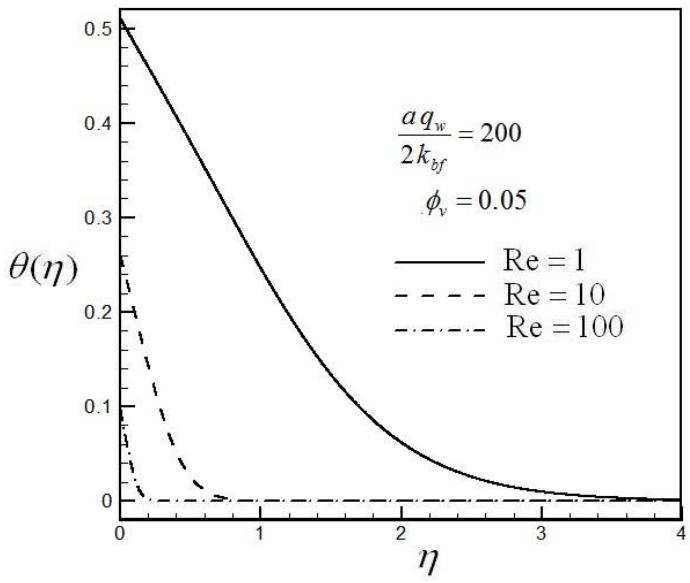

Fig. 6. Variation of $\theta(\eta)$ in terms of η at $\frac{aq_w}{2k_{bf}} = 200$ and $\phi_v = 0.05$ for different values of Reynolds number

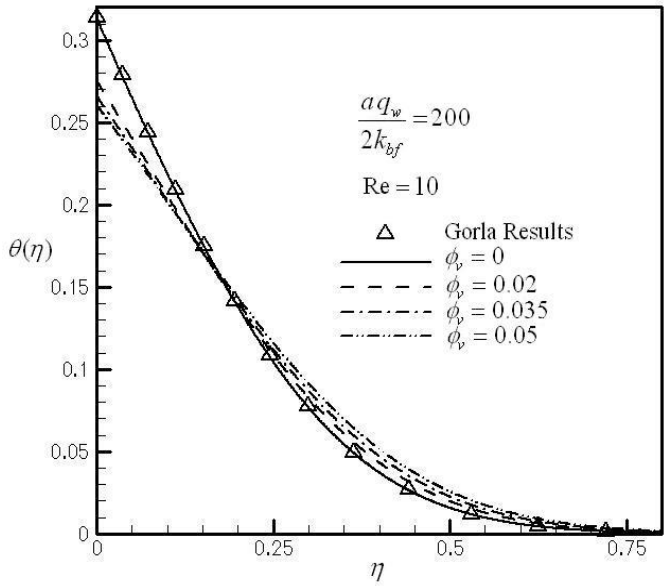

Fig. 7. Variation of $\theta(\eta)$ in terms of η at $\frac{aq_w}{2k_{bf}} = 200$ and Re=10 for different values of particle fractions

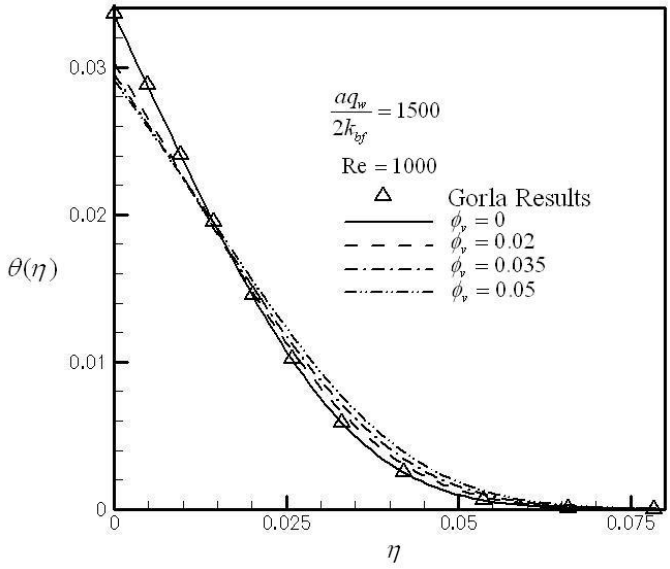

Fig. 8. Variation of $\theta(\eta)$ in terms of η at $\frac{aq_w}{2k_{bf}} = 1500$ and Re=1000 for different values of particle fractions

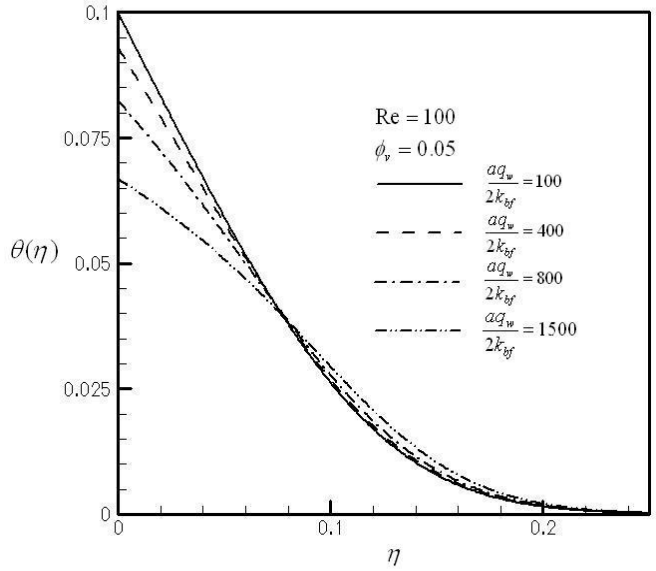

Fig. 9. Variation of $\theta(\eta)$ in terms of η at $\phi_v = 0.05$ and Re=100 for different values of $\frac{aq_w}{2k_{bf}}$

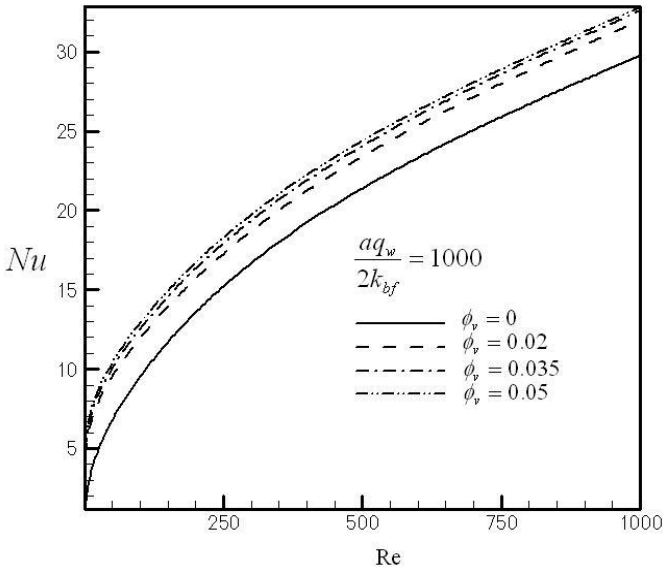

Fig. 10. Variation of Nusselt number in terms of Re at $\frac{a q_w}{2 k_{bf}} = 1000$ for different values of particle fractions

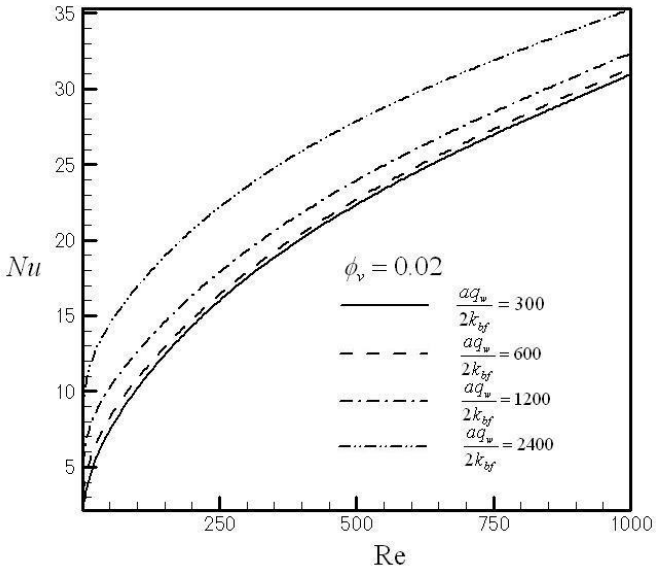

Fig. 11. Variation of Nusselt number in terms of Re at $\phi_v = 0.02$ for different values of $\frac{a q_w}{2 k_{bf}}$

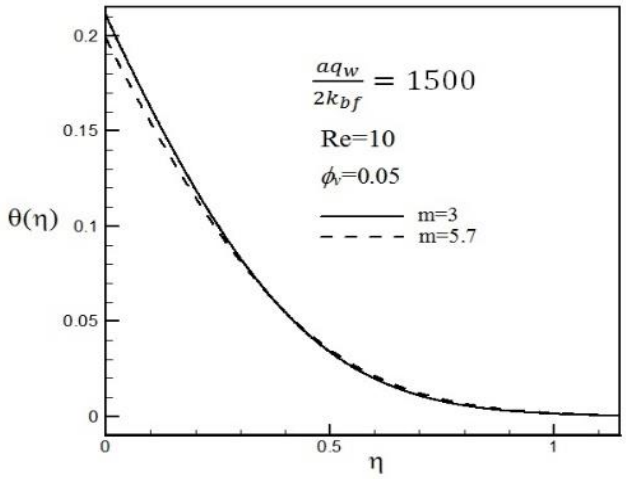

Fig. 12. Variation of $\theta(\eta)$ in terms of η at $\frac{a q_w}{2 k_{bf}} = 1500$ and Re=10 for different values of shape factor

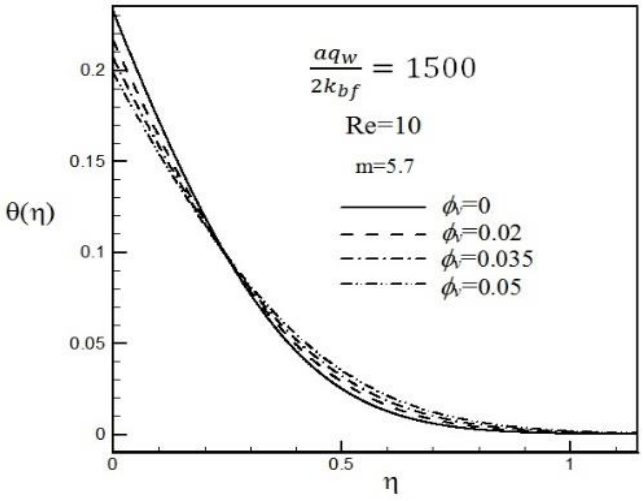

Fig. 13. Variation of $\theta(\eta)$ in terms of η at $\frac{a q_w}{2 k_{bf}} = 1500$ and Re=10 for different values of particle fractions

Table1. Different parameters of nano-fluid and base fluid

Parameter	**Value**
Thermal conductivity of base fluid, k_f	0.6316 [W/m-K]
Thermal conductivity of nano particle, k_p	40 [W/m-K]
Specific heat of base fluid, $C_{p,f}$	4.181 [kJ/kg-K]
Specific heat of nano particle, $C_{p,p}$	0.765 [kJ/kg-K]
Density of base fluid, ρ_f	987.6 [kg/m3]
Density of nano particle, ρ_p	3600 [kg/m3]
Viscosity of base fluid, μ_f	0.000538 [kg/m-s]
Diameter of nano particle, d_p	44 nm
Diameter of base fluid molecule, d_f	0.384 nm

Table2. The values of shape factor of different shapes of nanoparticles [2].

m			
	Spherical		3
	Platelet		5.7
	Cylinder		4.8
	Brick	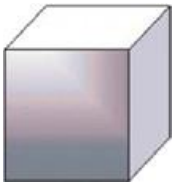	3.7

Appendix:

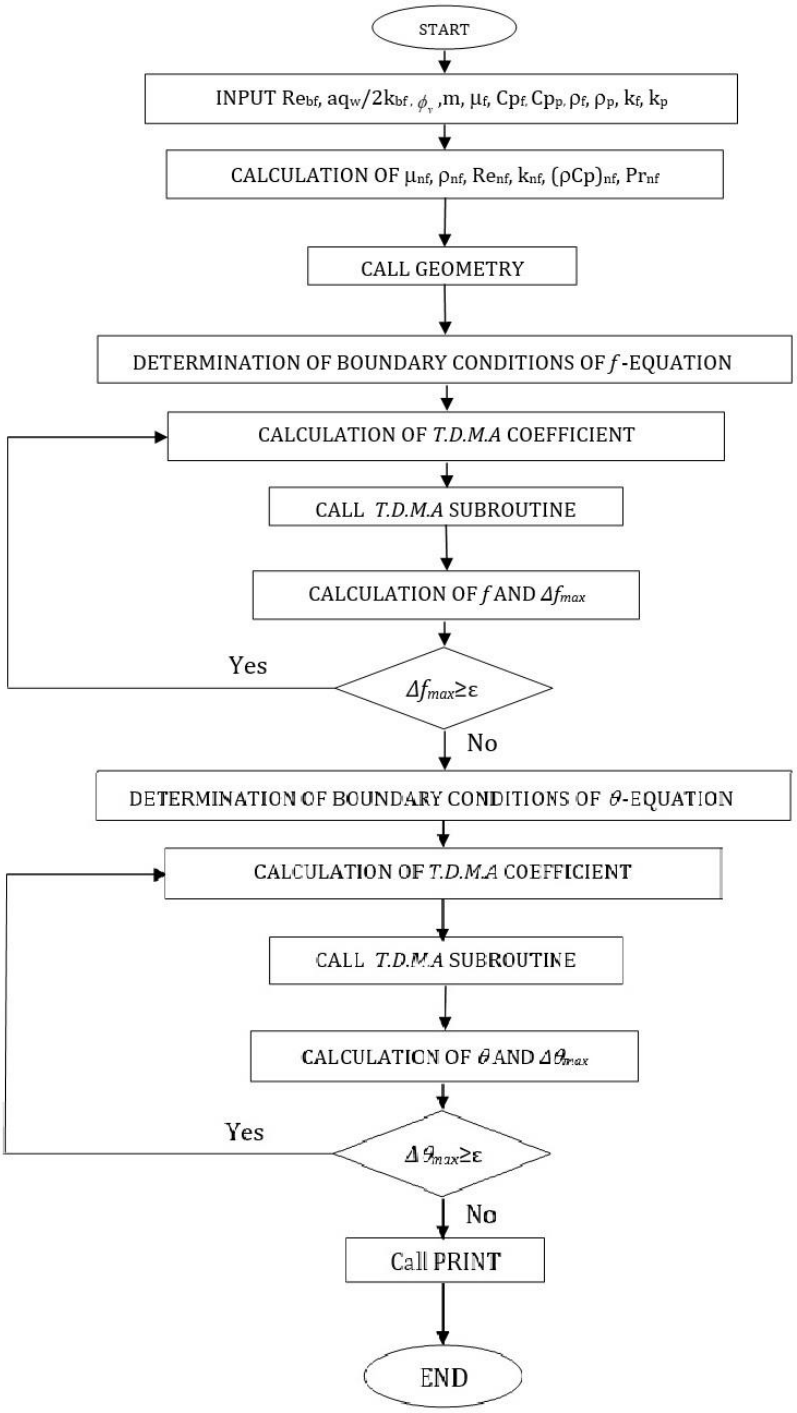
START
INPUT Re_{bf}, $aq_w/2k_{bf}$, ϕ_v, m, μ_f, Cp_f, Cp_p, ρ_f, ρ_p, k_f, k_p
CALCULATION OF μ_{nf}, ρ_{nf}, Re_{nf}, k_{nf}, $(\rho Cp)_{nf}$, Pr_{nf}
CALL GEOMETRY
DETERMINATION OF BOUNDARY CONDITIONS OF f-EQUATION
CALCULATION OF T.D.M.A COEFFICIENT
CALL T.D.M.A SUBROUTINE
CALCULATION OF f AND Δf_{max}
Yes
$\Delta f_{max} \geq \varepsilon$
No
DETERMINATION OF BOUNDARY CONDITIONS OF θ-EQUATION
CALCULATION OF T.D.M.A COEFFICIENT
CALL T.D.M.A SUBROUTINE
CALCULATION OF θ AND $\Delta \theta_{max}$
Yes
$\Delta \theta_{max} \geq \varepsilon$
No
Call PRINT
END